IEEE Access
Multidisciplinary | Rapid Review | Open Access Journal

Received March 13, 2019, accepted March 25, 2019, date of publication April 3, 2019, date of current version April 16, 2019.

Digital Object Identifier 10.1109/ACCESS.2019.2909070

Eight-Port MIMO Array Using Characteristic Mode Theory for 5G Smartphone Applications

YING LIU[1], (Senior Member, IEEE), AIDI REN[1], HU LIU[2], HANYANG WANG[3], (Senior Member, IEEE), AND CHOW-YEN-DESMOND SIM[4], (Senior Member, IEEE)

[1]Science and Technology on Antenna and Microwave Laboratory, Xidian University, Xi'an 710071, China
[2]Academy of Space Electronic Information Technology, Xi'an 710071, China
[3]Huawei Technologies Company, Ltd., Reading RG2 6UF, U.K.
[4]Department of Electrical Engineering, Feng Chia University, Taichung 40724, Taiwan

Corresponding author: Ying Liu (liuying@mail.xidian.edu.cn)

This work was supported by the National Natural Science Foundation of China (No.61871309) and Huawei Technologies Company Ltd., China.

ABSTRACT An 8-port multiple-input multiple-output (MIMO) array operating in the long-term evolution (LTE) band 42 (3400–3600 MHz) based on the characteristic mode theory (CMT) is described. As designing a multi-antenna system with multiple significant modes is difficult for the CMT, a new method is, therefore, proposed to effectively provide useful physical insights and improve the envelope correlation coefficient (ECC). Although many of the same modes are excited by two antennas, the proposed method is still effective to improve the ECC of the two antennas. A detailed and reasonable framework adopting the CMT to analyze geometries with multi-significant modes is presented. The consideration of the mode number can be avoided by using this method. For an arbitrary structure, it is verified that the modal weighting coefficient (MWC) phases of the same modes excited by two ports are in phase or out of phase. Therefore, for the design of a multi-port MIMO array, the same modes excited by different ports can be divided into two types: equiphase modes and antiphase modes in the proposed method, and the tradeoff of the equiphase modes and the antiphase modes is first proposed and analyzed as an efficient way to improve the ECC. Furthermore, the proposed method can also be applied to asymmetric structures. In order to prove the effectiveness of the proposed method in the design of MIMO antennas with desirable ECC, an 8-port MIMO array for 5G mobile applications is implemented and measured.

INDEX TERMS Multiple-input multiple-output (MIMO), characteristic modes, 5G mobile application.

I. INTRODUCTION

In the past decade, there has been an increasing demand to further enhance the channel capacity and spectrum efficiency of mobile communication. To achieve that, the MIMO technology is one of the best solutions at the moment. However, high correlation between signals in two different receivers may mitigate the channel capacity for a practical MIMO system. Thus, a performance metric known as the ECC has been widely used to evaluate the similarity between two antenna far-field patterns. For the case where low ECC is measured between antenna patterns, it means that uncorrelated incoming signals and high channel capacity can be achieved. At present, there are more than 6 or 8 antennas arranged in a mobile terminal for 5G mobile communication applications. Due to limited available spaces in smart phone, these antennas (formed as an array type) have to be arranged in such a way that the spacing between two adjacent antennas is very much lower than the theoretical 0.5 λ_0. Therefore, it is a challenging task for antenna engineers to satisfy and maintain the isolation and ECC performances.

Many efforts have been devoted to improve the MIMO performance after the allocation of the frequency spectrum (3.4-3.6 GHz) for future 5G wireless communication at the World Radio Communication Conference 2015 [1]. In [2], an eight-element antenna array working in the 3.5-GHz band was designed with good effective diversity gain in both uniform and non-uniform environment. However, this antenna array has occupied too much space and limited rooms are available for any other 4G antennas. Several compact multi-element antenna arrays for 3.5-GHz LTE MIMO operation in the smartphone have also been reported in [3]–[6].

The associate editor coordinating the review of this manuscript and approving it for publication was Fang Yang.

Neutralization line was used to realize acceptable isolation between adjacent antennas [3]–[5], which results in the increased complexity of the MIMO system. In [5], a hybrid multi-antenna array composed of 4G and 5G antenna modules is proposed, in which a bending monopole strip has served as the main radiator of the 5G array. Here, the measured isolations between adjacent antenna elements were slightly better than 10 dB. In comparison, the work in [6] has exhibited better isolation and ECC performances, but this design is not suitable for handset with a metal frame. In [7], an eight-port orthogonally dual-polarized antenna array is proposed. The array design is composed of a C-shaped coupled-fed antenna array and an L-shaped monopole slot antenna array, which realizes good isolation. Because this proposed MIMO array has a three-dimensional configuration, it will increase the difficulty and cost of manufacture. Furthermore, it is not suitable for metal-rimmed smartphone design.

The CMT was first proposed by Garbacz in 1965 [8]. In recent years, many researchers have paid attention to CMT because of the booming development of smartphones [9]. One of the most attractive properties of CMT is the orthogonality of characteristic fields over the radiation sphere at infinity. By taking advantage of this property, the CMT is therefore widely adopted in the mobile terminal with multi-antenna system, because good ECC performance can be realized.

As reported in [10]–[13], a new concept that can effectively realize multi-antenna system by exciting different modes via a smartphone chassis is presented. By using the CMT, the isolation between two elements can be improved, even though the distance between the two adjacent elements was decreased [14], [15]. At below 1 GHz, more than one resonant mode can be found by changing the structure of the smartphone chassis. The isolation and ECC of the multi-antenna system can be improved effectively by exciting different resonant modes [16], [17]. In [18], the optimal position of diversity antennas was studied by using CMT, when the location of the main antenna was given on the same mobile terminal. Multi-port antenna architecture with good isolation has also been designed by using CMT [19], [20], in which a two port MIMO antenna with good features was achieved by controlling the orthogonal characteristic modes below 1 GHz [21].

The theory of characteristic mode (TCM) was used to analyze the behavior of DGS (defected ground structures) and to improve the isolation by blocking the coupling modes [22], [23]. However, the DGS method cannot be used to improve the isolation when the current distributions on the edge and side of the chassis are nearly the same for coupling and uncoupling modes. Notably, the proposed method can deal with structures that have many significant modes, and it is still useful when the current distributions of many significant modes are similar. The antennas effects on the distributing currents of mobile chassis for frequency above 2 GHz have been studied by using the TCM, and it was verified that small antenna elements have greater impact on the characteristic modes of the chassis [24]. The TCM can also be used to design broadband antenna. In [25], broadband slotted planar antennas have been proposed by using the TCM, in which selective excitation of characteristic mode was further exploited by analyzing a common-fed and differential-fed capacitive-coupled circular aperture antenna. In [22]–[25], even though the TCM was exploited at frequency greater than 1 GHz, its corresponding ECC are not studied in these papers. Currently, to obtain desirable ECC, the TCM is always employed to analyze the structure and find the optimal placement of multi-antenna so that the modes excited by the different antennas are completely different. However, this method is not suitable for multi-antenna systems with multiple modes. Nevertheless, the proposed method can improve the ECC effectively by utilizing the existence of multiple significant modes, which is not found in any other papers.

In this paper, an 8-port MIMO array operating in LTE band 42 is proposed based on the CMT. Even though the structures with multiple modes are difficult to analyze via the CMT, the CMT adopted in this case can effectively improve the ECC of the MIMO array. The proposed method can be applied to the case that many of the same modes are excited by two antennas. The main purpose of this paper is to provide a reasonable framework that can utilize the CMT to design multi-antenna systems with multiple significant modes. In this paper, the basic theory of the proposed method is given. According to the theoretical analysis, for an arbitrary structure, it is verified that the MWC phases of the same modes excited by two ports are in phase or out of phase. This is an important property for the proposed method. A detailed analysis and design process is presented as follows; (1) appropriate antenna elements (eg. eight antenna elements) are selected, (2) the optimal placement of the antenna elements is determined by using the CMT, (3) the same modes excited by two antennas can be categorized into two modal types, namely, equiphase modes and antiphase modes, by denoting the difference of the MWC phase. Notably, the tradeoff of the equiphase modes and antiphase modes is realized to be an efficient way to improve the ECC, which has never been analyzed nor reported elsewhere. According to the physical insights provided by the CMT, some methods can improve the balance of the equiphase modes and antiphase modes, in which better ECC can be obtained. To prove this method, an 8-port MIMO array for 5G smartphone applications is utilized, and it is further validated that the CMT is effective in achieving good correlation performance at frequencies with multi-significant modes.

This paper is organized as follows; Section II describes the basic theory of the proposed method. In Section III, an 8-port MIMO array is proposed and the CMT is used to improve the performance of the MIMO array. Section IV presents the characterization of a fabricated prototype of the proposed array. Finally, a conclusion is given in Section V.

II. BASIC THEORY OF THE METHOD

Classical theory of characteristic modes for perfectly electrically conducting bodies (PEC) is based on the electric field

integral equation (EFIE) and the method of moment (MoM) [26], [27]. The characteristic modes of an arbitrary PEC can be derived from the generalized eigenvalue equation

$$\mathbf{X}\mathbf{J}_n = \lambda_n \mathbf{R}\mathbf{J}_n \tag{1}$$

where X and R are the imaginary and real parts of an impedance matrix Z. $\mathbf{J}_n$ and λ_n represent the eigenvector and eigenvalue of the n-th mode, respectively. The excited currents on a PEC body via an exciter can be expanded by a superposition of the characteristic currents:

$$\mathbf{J} = \sum_n \alpha_n \mathbf{J}_n \tag{2}$$

and the far-fields of the excited currents can be denoted by a linear superposition of the characteristic fields:

$$\mathbf{E} = \sum_n \alpha_n \mathbf{E}_n \tag{3}$$

$$\mathbf{H} = \sum_n \alpha_n \mathbf{H}_n \tag{4}$$

$$\alpha_n = \left\langle \mathbf{E}^i_{\tan}(\mathbf{r}), \mathbf{J}_n \right\rangle \Big/ (1 + j\lambda_n) \tag{5}$$

where α_n is the complex MWC of the corresponding mode. The magnitude of MWC represents the contribution of the corresponding mode in total radiation.

In this paper, the magnitude and phase of MWC are important factors for the following analysis, thus a brief analysis of the MWC phase of a multi-port structure is necessary. Here, the characteristic current $\mathbf{J}_n$ is real, so the phase of the MWC is determined by external excitation and the mode itself from (5). In order to analyze this problem more clearly, a delta-gap feed model for the planar antenna is considered.

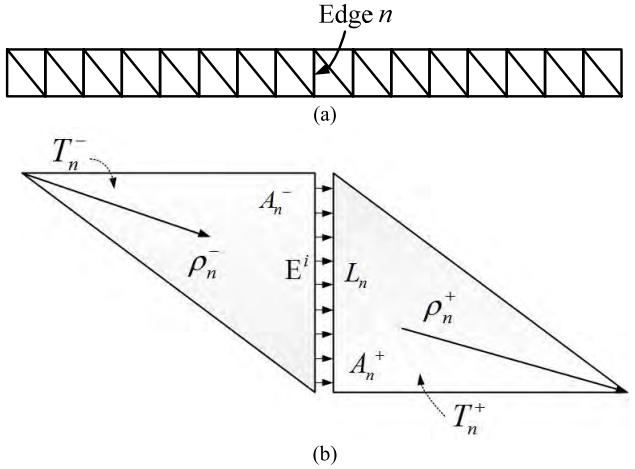

FIGURE 1. Delta-gap feed model. (a) Dipole antenna. (b) Delta gap at an edge.

The delta-gap feed model in the method of moment [28] is shown in Fig. 1. To be brief, a printed dipole illustrated in Fig. 1(a) is considered. The dipole is modeled by dividing the surface into many triangular elements and Rao-Wilton-Glisson (RWG) basis function is defined on the triangular elements. Here, the RWG basis function is defined over two adjacent triangles [29], as illustrated in Fig. 1(b). An RWG function can be expressed as:

$$\mathrm{f}_n^{\pm}(r) = \begin{cases} \dfrac{L_n}{2A_n^{\pm}}\rho_n^{\pm}, & r \in T_n^{\pm} \\ 0, & r \notin T_n^{\pm} \end{cases} \tag{6}$$

where T_n^+ and T_n^- are two triangles that share a common edge n, L_n is the length of the common edge n, A_n^+ and A_n^- are the area of the two triangles, ρ_n^+ is the vector toward the free vertex of T_n^+, and ρ_n^- is the vector from the free vertex of T_n^-.

The dipole is divided into two halves along the edge n. Edge n is the common edge of the two triangles. There is a voltage generator across the gap with a very small width between the two triangles, as shown in Fig. 1(b). The magnitude and phase of the voltage generator are V_n and 0°. Then, the electric field between the small gap can be expressed as [28]:

$$\mathbf{E}^i = V_n / d\hat{\mathbf{n}} \tag{7}$$

where d is the width of the gap and the vector $\hat{n}$ is normal to edge n. For an arbitrary antenna, if there is only one Rao-Wilton-Glisson (RWG) element n with a voltage generator, the electric field will be zero everywhere except for the RWG element n. Characteristic current can be expanded as:

$$\mathbf{J}_n = \sum_i I_i \mathbf{f}_i \tag{8}$$

where $\mathbf{f}_i$ is RWG basis function, and I_i is the weighting coefficient for the i-th basis function. Inserting (7) and (8) into (5), and considering the fact that the vertical component of the RWG function $\mathbf{f}_n$ equals one along the edge, then the following equation can be obtained:

$$\begin{aligned} \alpha_n &= \frac{\left\langle \mathbf{E}^i_{\tan}(\mathbf{r}), \mathbf{J}_n \right\rangle}{1 + j\lambda_n} = \frac{\int_{\mathbf{f}_n} V_n / d\hat{\mathbf{n}} \cdot I_n \mathbf{f}_n d\mathbf{r}}{1 + j\lambda_n} \\ &= \frac{\int_{\mathbf{f}_n} |\mathbf{f}_n| \left| V_n / d\hat{\mathbf{n}} \right| \cdot \cos\theta \cdot I_n d\mathbf{r}}{1 + j\lambda_n} = \frac{\pm L_n V_n I_n}{1 + j\lambda_n} \end{aligned} \tag{9}$$

where θ is the angle between vector $\mathbf{E}^i$ and $\mathbf{f}_n$.

In order to give a brief analysis of the MWC phase of a multi-port structure, an arbitrary two-port structure is considered. For the two-port structure, when one port is excited, the other one is matched with a 50 Ω load. In the case of port 1 working, there is only RWG element n with a voltage generator and the phase of the generator is zero. In the case of port 2 working, there is only RWG element m with a voltage generator and the phase is also zero. For the same characteristic mode n, the MWC excited by the two ports can be expressed as:

$$\alpha_{n-port1} = \frac{\left\langle \mathbf{E}^i_{\tan}(\mathbf{r}), \mathbf{J}_n \right\rangle}{1 + j\lambda_n} = \pm \frac{L_n V_n I_n}{1 + j\lambda_n} \tag{10}$$

$$\alpha_{n-port2} = \frac{\left\langle \mathbf{E}^i_{\tan}(\mathbf{r}), \mathbf{J}_n \right\rangle}{1 + j\lambda_n} = \pm \frac{L_m V_m I_m}{1 + j\lambda_n} \tag{11}$$

Observing (10) and (11), $L_n V_n I_n$ and $L_m V_m I_m$ are real. For the same characteristic mode n, the eigenvalue λ_n in (10) and

(11) is equal. When the signs of (10) and (11) are the same, the MWC phases of the two ports are in phase, otherwise the MWC phases of the two ports are out of phase. It is verified that the MWC phases of the same modes excited by two ports are in phase or out of phase. This property is very important for the following analysis. Owing to this property, the proposed method is also appropriate for asymmetric structures.

The most attractive property of the characteristic modes is the orthogonality of the characteristic fields in the far field. This property can be presented as:

$$\oiint_S \mathbf{E}_m \cdot \mathbf{E}_n^* dS = \eta \delta_{nm} \tag{12}$$

where $\mathbf{E}_n$ and $\mathbf{E}_m$ are the characteristic electric fields of the n-th and m-th modes, respectively. This property is significant for the MIMO design. Envelope correlation is an important factor for channel capacity and it can be expressed by far-field patterns [30]:

$$\rho_e(i,j) = \frac{\left| \iint_{4\pi} \left[F_i(\theta,\phi) \cdot F_j^*(\theta,\phi) \right] d\Omega \right|^2}{\iint_{4\pi} |F_i(\theta,\phi)|^2 d\Omega \cdot \iint_{4\pi} \left| F_j(\theta,\phi) \right|^2 d\Omega} \tag{13}$$

where $F_i(\theta,\phi)$ and $F_j(\theta,\phi)$ are the far-field patterns of the i-th and j-th antennas. The far-field pattern of the i-th antenna can be expressed as a linear superposition of the characteristic fields:

$$F_i(\theta,\phi) = \sum_{n=1}^{N} \alpha_{n,i} \mathbf{E}_n(\theta,\phi) \tag{14}$$

where $\alpha_{n,i}$ is the complex MWC of the n-th mode excited by the i-th antenna. In the light of (12), (13) and (14), the formulation can be derived as [30]:

$$\rho_e(i,j) = \frac{\left| \sum_{n=1}^{N} \alpha_{n,i} \alpha_{n,j}^* \right|^2}{\left(\sum_{n=1}^{N} |\alpha_{n,i}|^2 \right) \left(\sum_{n=1}^{N} |\alpha_{n,j}|^2 \right)} \tag{15}$$

The smaller the numerator of (15) is, the smaller the envelope correlation. Only if the numerator of (15) equals zero, then the envelope correlation is minimized. In the process of analyzing the multi-antenna system by CMT, there are two common conditions:

The modes excited by the i-th and j-th antennas are completely different.

The modes excited by the i-th and j-th antennas are overlapped.

In the first condition, the numerator of (15) is equal to zero, then the envelope correlation equals zero. At present, many designs of multi-antenna systems are based on this condition. The TCM is employed to analyze the structure and find the optimal placement of multi-antenna so that the modes excited by the different antennas are completely different. However, this method is only effective for the case when there are only a few significant modes.

In the second condition, many of the same modes are excited by different antennas. When the structures possess multi-significant modes, the second condition is common. In this paper, attention has been paid to this condition because the structure of the ground plane with a metal bezel owns many significant modes at frequencies working between 3.4 and 3.6 GHz. Here, a new method is proposed to achieve low envelope correlation under these circumstances. For example, in a two-antenna system, the fields produced by Ant 1 and Ant 2 can be expressed as a linear superposition of the characteristic fields:

$$\begin{aligned} \mathbf{E}_{Ant1} = {} & \alpha_{1,1}\mathbf{E}_1 + \ldots + \alpha_{M,1}\mathbf{E}_M + \alpha_{C_1,1}\mathbf{E}_{C_1} \\ & + \ldots + \alpha_{C_{N1},1}\mathbf{E}_{C_{N1}} \end{aligned} \tag{16}$$

$$\begin{aligned} \mathbf{E}_{Ant2} = {} & \alpha_{1,2}\mathbf{E}_1 + \ldots + \alpha_{M,2}\mathbf{E}_M + \alpha_{D_1,2}\mathbf{E}_{D_1} \\ & + \ldots + \alpha_{D_{N2},2}\mathbf{E}_{D_{N2}} \end{aligned} \tag{17}$$

where $\alpha_{n,1}$ and $\alpha_{n,2}$ denote the MWC of the n-th mode excited by Ant 1 and Ant 2, respectively. The first M modes are the same modes excited by Ant 1 and Ant 2. The collection of modes $\{C_1, C_2, \ldots C_{N1}\}$ and $\{D_1, D_2, \ldots D_{N2}\}$ represents the completely different modes excited by Ant 1 and Ant 2, respectively. Substituting (16) and (17) into the numerator of (15) and considering the orthogonality of the characteristic fields in the far field, we find:

$$\begin{aligned} & \left| \sum_{n=1}^{M+N1+N2} \alpha_{n,i} \alpha_{n,j}^* \right|^2 \\ & \quad = \left| \alpha_{1,1}\alpha_{1,2}^* + \alpha_{2,1}\alpha_{2,2}^* + \ldots + \alpha_{M,1}\alpha_{M,2}^* \right|^2 \end{aligned} \tag{18}$$

The same modes excited by the two antennas can be divided into equiphase modes and antiphase modes by the difference of the MWC phase according to the analysis above. Equiphase modes indicate that the MWCs of the same modes excited by the two antennas are in phase. Antiphase modes indicate that the MWCs of the same modes are out of phase. Taking consideration of the equiphase modes and antiphase modes, (18) can be rewritten as:

$$\begin{aligned} & \left| \sum_{n=1}^{P+Q} \alpha_{n,i} \alpha_{n,j}^* \right|^2 \\ & \quad = \Big| \left|\alpha_{E1,1}\right| \left|\alpha_{E1,2}\right| e^{je_1} e^{-je_1} + \ldots + \left|\alpha_{EP,1}\right| \left|\alpha_{EP,2}\right| \\ & \qquad \times e^{je_P} e^{-je_p} + \left|\alpha_{A1,1}\right| \left|\alpha_{A1,2}\right| e^{ja_1} e^{-j(a_1+\pi)} \\ & \qquad + \ldots + \left|\alpha_{AQ,1}\right| \left|\alpha_{AQ,2}\right| e^{ja_Q} e^{-j(a_Q+\pi)} \Big|^2 \\ & \quad = \Big| \left(\left|\alpha_{E1,1}\alpha_{E1,2}\right| + \ldots + \left|\alpha_{EP,1}\alpha_{EP,2}\right|\right) \\ & \qquad - \left(\left|\alpha_{A1,1}\alpha_{A1,2}\right| + \ldots + \left|\alpha_{AQ,1}\alpha_{AQ,2}\right|\right) \Big|^2 \\ & \quad = |\text{EC-AC}|^2 \end{aligned} \tag{19}$$

$$\begin{aligned} \text{EC} & \\ & = \left|\alpha_{E1,1}\alpha_{E1,2}\right| + \ldots + \left|\alpha_{EP,1}\alpha_{EP,2}\right| \end{aligned} \tag{20}$$

$$\text{AC} = \left|\alpha_{A1,1}\alpha_{A1,2}\right| + \ldots + \left|\alpha_{AQ,1}\alpha_{AQ,2}\right| \quad (21)$$

where $\alpha_{En,1}$ and $\alpha_{En,2}$ denote the corresponding MWC of the n-th equiphase modes excited by Ant 1 and Ant 2, respectively. $\alpha_{An,1}$ and $\alpha_{An,2}$ denote the n-th MWC of antiphase modes excited by Ant 1 and Ant 2, respectively. P and Q are the number of equiphase modes and antiphase modes, respectively. EC (Equiphase Mode Coefficient) is the summation of the product of the MWC of the excited equiphase modes by the two antennas. AC (Antiphase Mode Coefficient) is the summation of the product of the MWC of the excited antiphase modes by the two antennas.

Obviously, (15) and (19) will be minimized as long as EC equals AC. To obtain a better ECC, EC can be made close enough to the AC by changing the weightings of the equiphase modes and antiphase modes. The physical insights provided by the CMT can be used to reduce the difference between EC and AC.

In summary, low envelope correlation can be realized by the tradeoff of the equiphase modes and antiphase modes. By using this method, there is no need to completely excite different modes for different antennas. This proposed method is effective in designing multi-antenna systems with multiple significant modes.

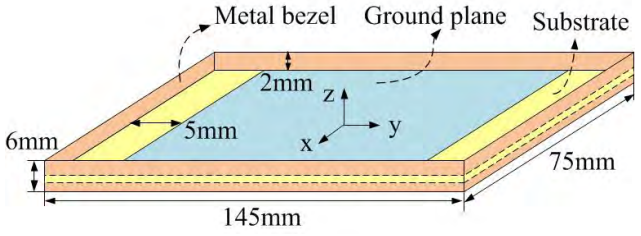

FIGURE 2. Geometry of the ground plane with a metal bezel.

III. THE EIGHT PORT MIMO ARRAY DESIGN

A. CHARACTERISTIC MODES ANALYSIS

In this sub-section, the ground (with a dielectric substrate) and metal bezel are analyzed by using the CMT. As shown in Fig. 2, the dimension of the ground plane is 135 mm $\times$ 75 mm, and the height of the metal bezel is 6 mm. The material of the dielectric substrate is FR4 and it has a thickness of 0.8 mm. Fig. 3 shows the corresponding modal significances (MS) of the first twenty characteristic modes obtained from the characteristic mode analysis. Significant modes and non-significant modes can be defined by MS. The characteristic modes with $MS \geq 1/\sqrt{2}$ can be regarded as significant modes [9]. It is known that up to 12 modes are significant modes across the bands of interest (3.4-3.6 GHz).

The mode current distribution of mode 1-20 at 3.4 GHz is shown in Fig. 4. In this figure, the main current flowing direction is denoted by black arrows, and the characteristic current is strong around the two ground clearances for most of the modes. As many modes will be excited if an antenna

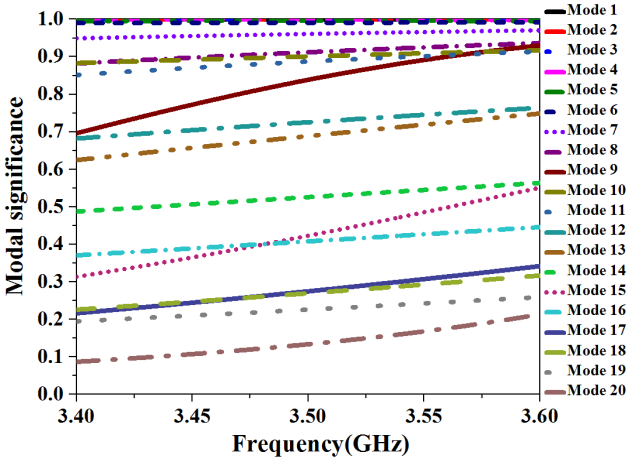

FIGURE 3. Modal significances obtained from CM.

is placed close to the ground clearances, it is more precise to reserve two clearances in the design of a 5G MIMO array and in the process of characteristic mode analysis. Because one can see that many modes will be excited, no matter where the exciter is placed, therefore, in this case, minimizing the envelope correlation by exciting completely different modes between different antennas is difficult to realize.

In view of this situation, two kinds of antenna elements are proposed to enhance the isolation, which are shown in Fig. 5. In Fig. 5(a), the black arrows indicate the main current flowing direction in the loop element. For the loop element, the excited modes are the ones with the flowing direction of the mode current in parallel to the longer side of the loop element [31]. The E-field distribution across the slot is shown in Fig. 5(b). As can be seen from (5), the modes will be effectively excited when the E-field direction of the external excitation is parallel to the flowing direction of the mode current. Thus, the slot element will mainly excite the modes that the mode current is perpendicular to the longer side of the slot.

According to the analysis above, these two kinds of antenna elements will excite two different types of mode currents. Thus, the isolation between the loop element and the slot element is desirable when the two elements are arranged as in Fig. 5(c). In this case, the two antenna elements mainly excite the current distribution on the ground that is mutually perpendicular.

B. MIMO ARRAY DESIGN

The locations of MIMO elements can be decided by applying the characteristic mode analysis. The longer side of loop elements and slot elements should be parallel to the longer side of the ground plane, while four elements are required to be arranged along one side of the ground plane. From Fig. 4, it is evident that the current flowing direction of nearly 20 modes on the shorter side of the ground plane is perpendicular to the longer side of the ground plane. Therefore, the locations of

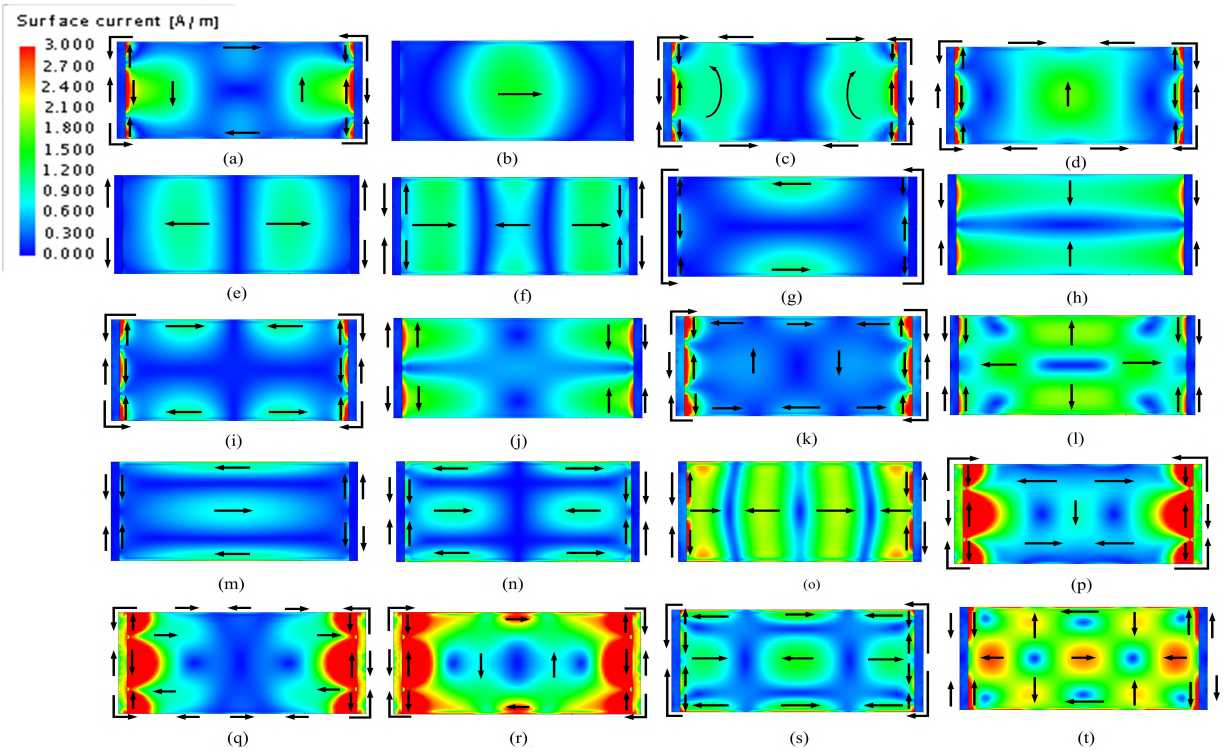

FIGURE 4. (a)-(t) Modal current distribution of mode 1-mode 20.

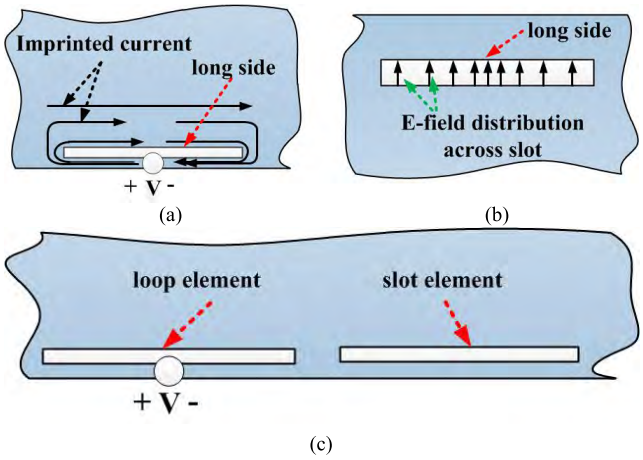

FIGURE 5. Geometry of the feeding structures. (a) Loop element. (b) Slot element. (c) The position of the two elements.

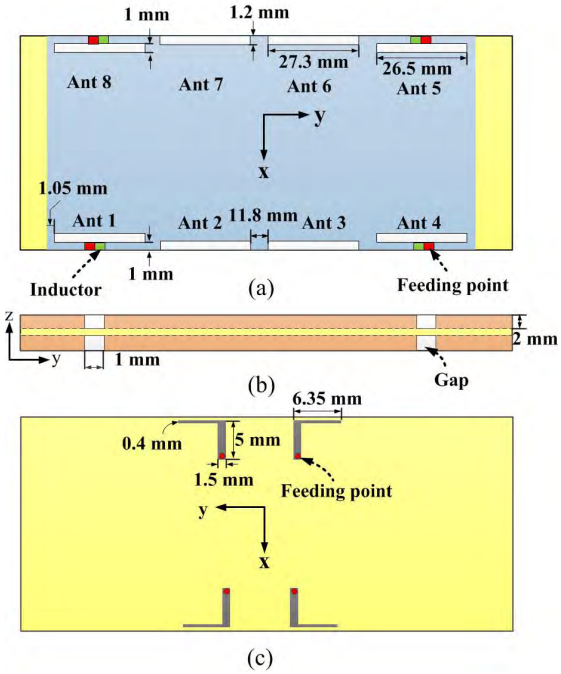

FIGURE 6. Configuration of the MIMO array. (a) Top view. (b) Side view. (c) Bottom view.

the loop elements should be in close proximity to the ground clearances in order to excite as fewer modes as possible.

Figure 6 shows the configuration of the 8-port MIMO array. Here, four identical slot antennas (Ants 2, 3, 6 and 7) are located at the center region of the ground plane, whereas four identical loop antennas (Ants 1, 4, 5 and 8) are arranged close to the ground clearances. By doing so, the 8-port MIMO array is now a symmetrical structure. In Fig. 6(a), the red and green color sections denote the feeding points of the loop antennas and the series inductors (9.1 nH), respectively, in which the inductors are incorporated to achieve better impedance matching. As shown in Fig. 6(b), four gaps are loaded into the metal bezel and they are located at each respective feeding point of the loop antennas. The existence of these four gaps can improve the impedance matching of the loop antennas as well. As depicted in Fig. 6(c), the printed L-shaped microstrip lines are used to excite the slot antennas.

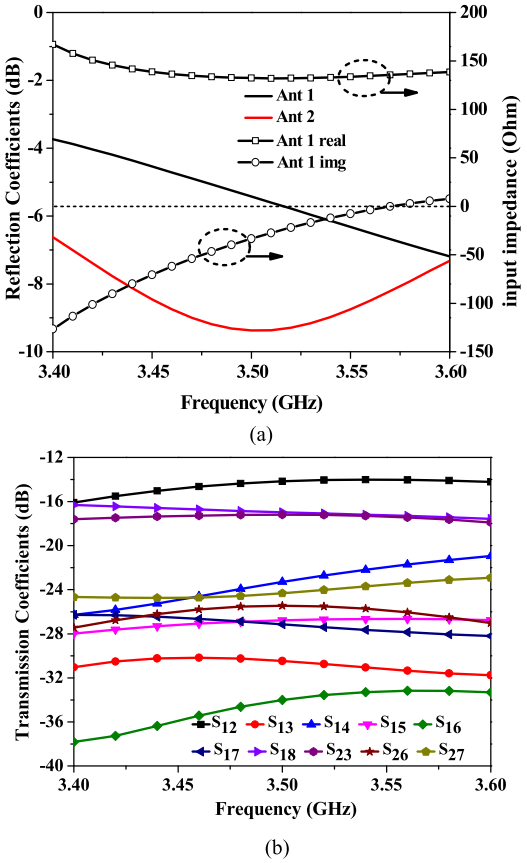

FIGURE 7. Simulated (a) reflection coefficients and input impedance of ant 1 and (b) transmission coefficients of the MIMO antennas.

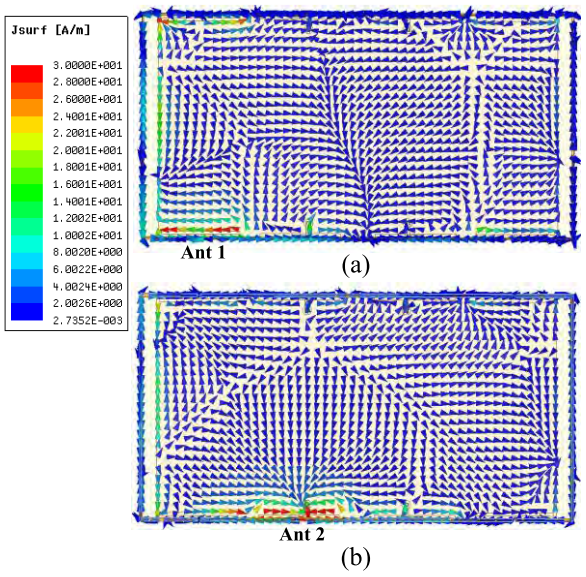

FIGURE 8. Simulated vector current distribution at 3.6 GHz. (a) Ant 1 excitation. (b) Ant 2 excitation.

Figure 7 shows the simulated S parameters of the MIMO array. In Fig. 7(a), a better impedance bandwidth is achieved by Ant 2 as compared with Ant 1. Interestingly, the imaginary input impedance of Ant 1 is zero at 3.57 GHz, meaning that Ant 1 may resonate at 3.57 GHz. In this case, even without any decoupling structure, the isolations between eight antennas are still better than 13.5 dB, as shown in Fig. 7(b). The simulated vector current distributions at 3.6 GHz when Ant 1 and Ant 2 are separately excited are shown in Fig. 8. The current flowing directions excited by Ant 1 (loop antenna) and Ant 2 (slot antenna) are mainly parallel to the longer side of the loop element and perpendicular to the longer side of the slot element, respectively. Thus, the above results have validated the effectiveness of the two types of MIMO elements. Fig. 9 shows that the simulated ECC value between Ant 1 and Ant 8 is 0.44 at 3.4 GHz, which is undesirable. The TCM is thus adopted to solve this problem and provide further physical insights.

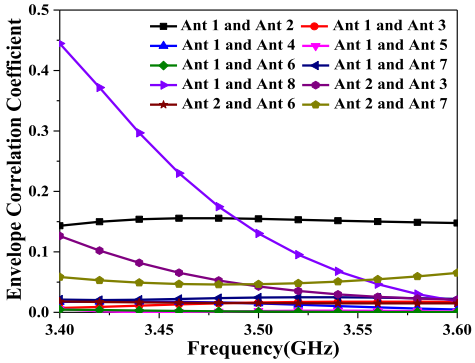

FIGURE 9. Simulated ECC of the MIMO array.

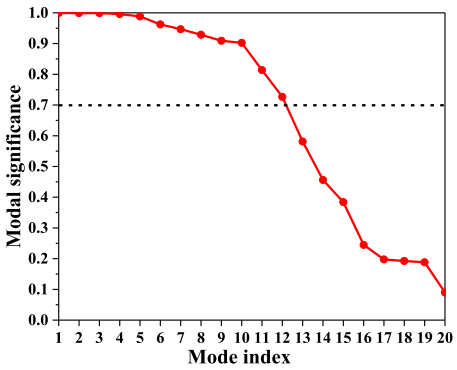

FIGURE 10. MS of the ground with antenna elements at 3.4 GHz.

The 8-port MIMO system is analyzed by using the CMT under the consideration of antenna effect. The MS of the chassis with MIMO elements at 3.4 GHz is shown in Fig. 10. Compared with Fig. 3, two additional significant modes are obtained by introducing MIMO elements at 3.4 GHz. The current distributions of first 20 modes at 3.4 GHz are sketched in Fig. 11. A comparison is performed between Fig. 4 and Fig. 11 to study the effect of antenna elements on chassis modes. It can be clearly observed that the current of most modes usually concentrates around the MIMO elements and ground clearances, but the overall current distributions of many ground modes are not significantly affected. The corresponding characteristic modes of the chassis (with and

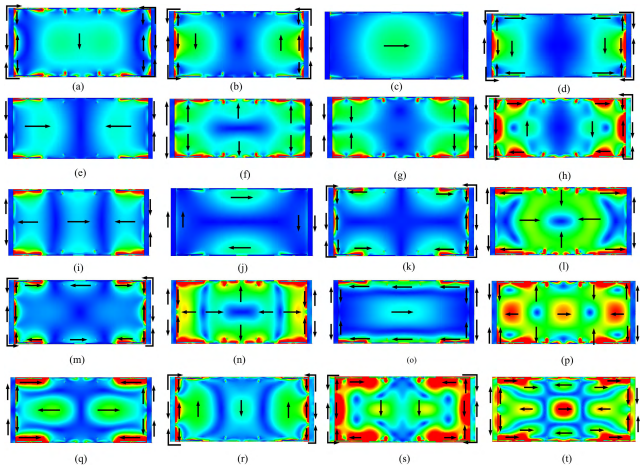

FIGURE 11. (a)-(t) Modal current distribution of mode 1-mode 20.

without loading MIMO element) are shown in Table 1. Here, chassis mode 17 has ceased to exist, whereas a new mode (mode 19) has appeared on the chassis with MIMO array. Based on the above results, one can realized that the introduction of MIMO elements will results in the variation of the MS associated to the chassis modes. Notably, during the analysis of TCM, only the first 20 modes with higher MS are investigated. Thus, the increase or decrease of MSs associated to ground modes may give rise to the appearance or disappearance of some modes. According to the analysis above, the introduction of antenna elements will affect the chassis modes, but the number of significant modes does not increase evidently.

TABLE 1. The corresponding characteristic modes excited on the chassis with and without loading MIMO element.

Chassis	Chassis with MIMO
Mode 1	Mode 2
Mode 2	Mode 3
Mode 3	Mode 4
Mode 4	Mode 1
Mode 5	Mode 5
Mode 6	Mode 9
Mode 7	Mode 10
Mode 8	Mode 6
Mode 9	Mode 11
Mode 10	Mode 7
Mode 11	Mode 13
Mode 12	Mode 12
Mode 13	Mode 15
Mode 14	Mode 18
Mode 15	Mode 14
Mode 16	Mode 18
Mode 17	-
Mode 18	Mode 8
Mode 19	Mode 20
Mode 20	Mode 16
-	Mode 19

The normalized magnitudes and phases of MWC when Ant 1 and Ant 8 are individually excited at 3.4 GHz are shown in Fig. 12. As shown in Fig. 12(a), the normalized MWC

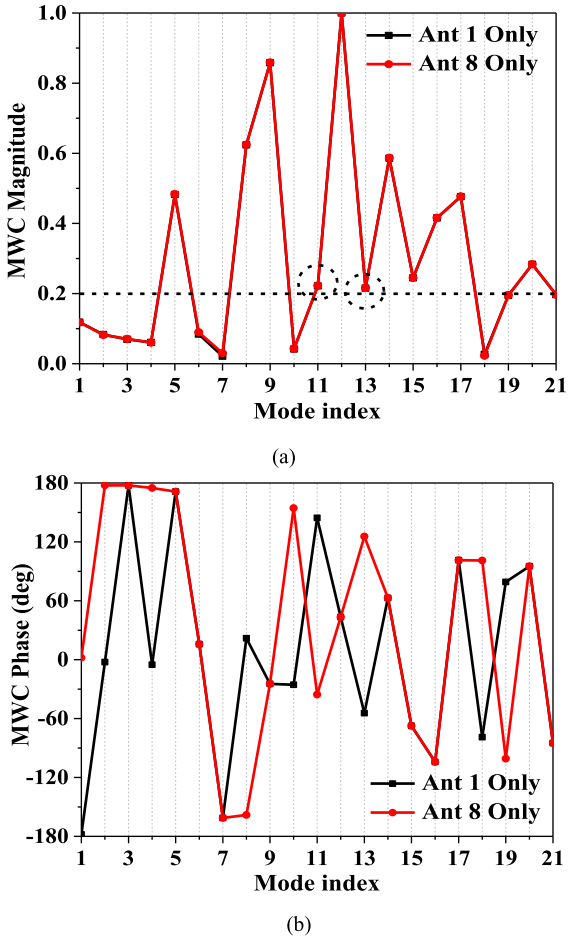

FIGURE 12. Simulated magnitude and phase of modal weighting coefficients at 3.4 GHz when Ant 1 and Ant 8 are separately excited. (a) Normalized magnitude. (b) Phase.

magnitudes of Ant 1 and Ant 8 are overlapped with each other, because the two antennas are located symmetrically with the same loop antenna type. Here, the modes with normalized magnitudes of MWC lower than 0.2 can be ignored, and only the main modes are considered [32]. Therefore, there are 11 identical main modes excited by Ant 1 and Ant 8. According to Fig. 12(b), among the excited main modes, the antiphase modes excited by the two antennas are mode 8, mode 11 and mode 13. The equiphase modes excited by the two antennas are mode 5, mode 9, mode 12, mode 14, mode 15, mode 16, mode 17 and mode 20. From the results presented in Fig. 12, the number of equiphase modes (excited by Ants 1 and 8) is far more than the antiphase modes. It is also noteworthy that the normalized MWC magnitudes of the antiphase modes (excited by Ants 1and 8) are smaller than the normalized MWC magnitudes of the equiphase modes. The simulated values from Fig. 12 can be applied to (20), (21) and (15), and the calculated EC, AC and ECC are 2.86, 0.48 and 0.51, respectively. From the calculated results, EC is greater than AC, while the ECC between Ant 1 and Ant 8 is undesirable. The calculated ECC between Ant 1 and Ant 8 from CMT is consistent with the simulated result from HFSS. Only

the main modes are under consideration during the analysis of the CMT; as a result, there are slight differences between the two results. As shown in Fig. 12 (a), among the antiphase modes excited by the two antennas, the normalized MWC magnitudes of modes 11 and 13 are very small; therefore, it is desirable to improve the excitation of mode 11 and mode 13. As a result, the value in (15) will be smaller than 0.51, and the ECC between Ant 1 and Ant 8 will be better than before.

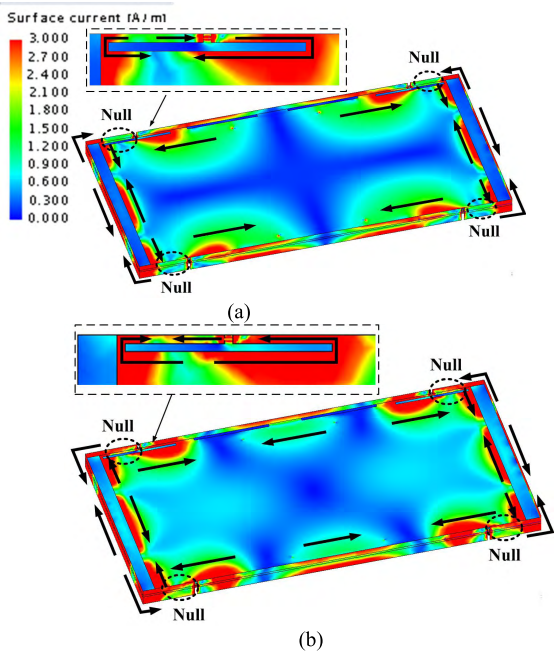

FIGURE 13. Modal current distribution of (a) mode 11 and (b) mode 13.

Figure 13 presents the modal current distribution of modes 11 and 13. Here, current nulls are observed around the loop antenna for both modes. Thus, the two modes cannot be well excited by the loop antenna based on the previous analysis of the loop antenna. In order to effectively excite both modes 11 and 13, the loop elements can be arranged near the center of the longer side of the ground plane. However, it will deteriorate the isolation between Ant 1 and Ant 2 owing to the very short distance between the two antennas. Thus, this method is not applicable for this design. Modifying the geometry of the MIMO system is another way to improve the excitation of modes 11 and 13. It is suggested that the modal current nulls of modes 11 and 13 should be far away from the loop antenna. Nevertheless, the changes of the geometry need to be very slight to create small effects on the other modes.

C. PROPOSED EIGHT-PORT MIMO ARRAY

The proposed MIMO array is designed according to the analysis above. Fig. 14 depicts the geometry of the proposed MIMO array. Compared to the initial MIMO array, the only difference is the metal bezel that has four additional gaps. To change the characteristic current of modes 11 and 13, these gaps are in close proximity to the shorter sides of the metal bezel, and they are located at the position with a maximum characteristic current of modes 11 and 13, as shown in Fig. 13.

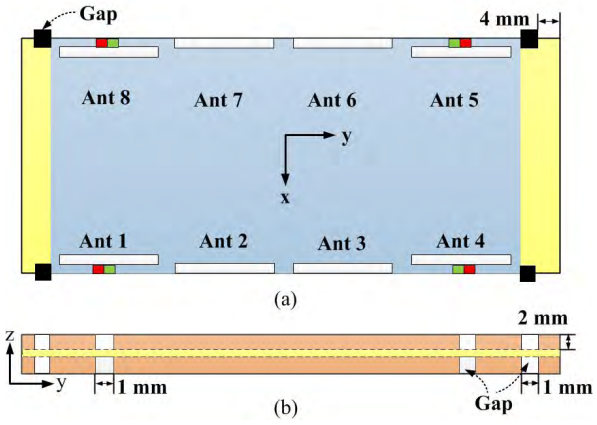

FIGURE 14. Configuration of the proposed MIMO array. (a) Top view. (b) Side view.

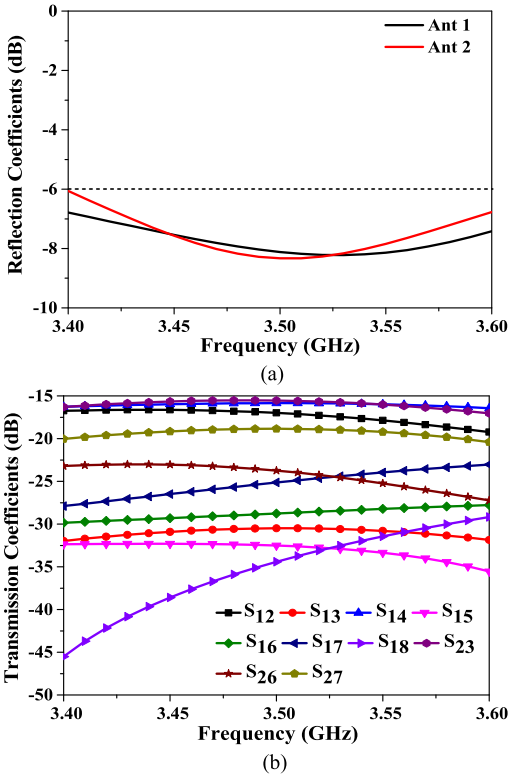

FIGURE 15. Simulated (a) reflection coefficients and (b) transmission coefficients of the proposed MIMO antenna.

The simulated S parameters of the proposed MIMO array are depicted in Fig. 15. The results account for the advantage of adding the four gaps. In this figure, the impedance matching of Ant 1 is improved and the port isolations of the MIMO antenna are better than 15.5 dB, due to the loading of these four gaps. It can be further observed from Fig. 16 that the ECCs of the MIMO array are lower than 0.14, which indicate great improvement compared with the initial MIMO array design when applying the characteristic mode method. The simulated ECC value between Ant 1and Ant 8 is very negligible at 3.4 GHz.

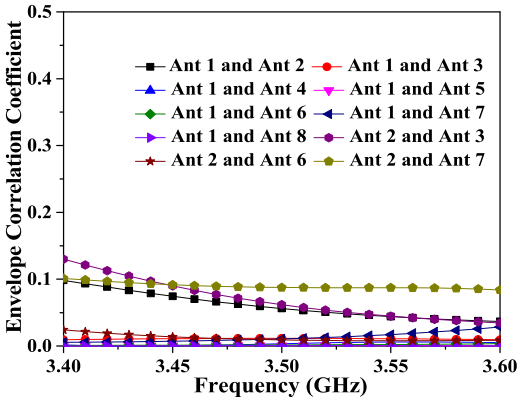

FIGURE 16. Simulated ECC of the proposed MIMO antenna.

TABLE 2. The correspondence of modes between the MIMO array with and without four gaps.

Ground with MIMO	Ground with MIMO and four gaps
Mode 1	Mode 1
Mode 2	Mode 2
Mode 3	Mode 3
Mode 4	-
Mode 5	Mode 4
Mode 6	Mode 6
Mode 7	Mode 7
Mode 8	Mode 10
Mode 9	Mode 8
Mode 10	Mode 9
Mode 11	Mode 11
Mode 12	Mode 12
Mode 13	Mode 13
Mode 14	Mode 14
Mode 15	Mode 15
Mode 16	Mode 18
Mode 17	Mode 17
Mode 18	Mode 5
Mode 19	-
Mode 20	Mode 20
-	Mode 16
-	Mode 19

On the basis of the previous analysis, the reason for the improvement of ECC (Ant 1 and Ant 8) is due to the effective excitation of antiphase modes. In order to validate the analysis, it is necessary to analyze the proposed MIMO array by using the CMT. The correspondence of modes between the MIMO array with and without loading the four gaps is shown in Table 2. For brevity, the mode current distribution of the MIMO array with four additional gaps is not shown. From Table 2, it is observed that mode 4 and mode 19 of the MIMO array have vanished due to the introduction of these four gaps. In addition, two new modes (mode 16 and mode 19) have appeared on the chassis owing to the introduction of these four gaps. By considering the four additional gaps, the current of most modes also concentrates around the MIMO elements and ground clearances. For the proposed MIMO array, the simulated magnitudes and phases of MWC at 3.4 GHz when Ant 1 and Ant 8 are individually excited are shown in Fig. 17.

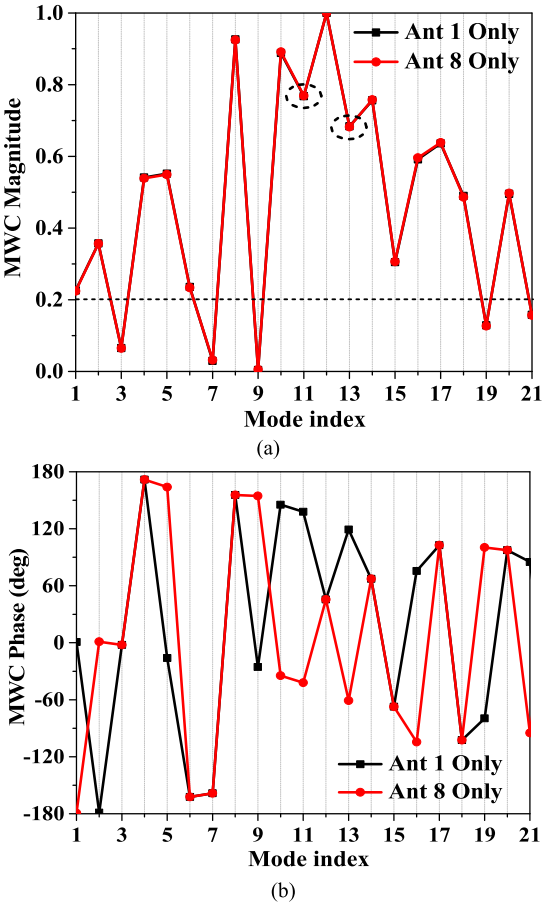

FIGURE 17. Simulated magnitude and phase of modal weighting coefficients of the proposed MIMO array at 3.4 GHz when Ant 1 and Ant 8 are excited, respectively. (a) Normalized magnitude. (b) Phase.

Here, 16 main modes are excited by Ant 1 and Ant 8, and amid these main excited modes, the antiphase modes excited by the two antennas are mode 1, mode 2, mode 5, mode 10, mode 11, mode 13 and mode 16. By further observing Fig. 17, the equiphase modes excited by the two antennas are mode 4, mode 6, mode 8, mode 12, mode 14, mode 15, mode 17, mode 18 and mode 20. For Ant 1 and Ant 8, the normalized MWC magnitudes of mode 11 and mode 13 excited by them are comparable and their values are 0.77 and 0.68, respectively. Fig. 18 presents the modal current distributions of modes11 and 13. The modal current distributions around the loop antenna without current nulls indicate that mode 11 and mode 13 can be excited very well by Ant 1 and Ant 8. From Fig. 18, it is obvious that the additional gaps have a small effect on modal current distribution. As can be seen in Fig. 17, the number of antiphase modes is increased after loading the four gaps. Here, almost all of the excitation of antiphase modes is improved and the results are the same with the improvement of mode 11 and mode 13. Equations (20), (21) and (15) can also be calculated according to the simulated results yielded in Fig. 17, and the calculated EC, AC and ECC are 3.77, 2.68 and 0.028, respectively, in which the EC value is now nearer to AC. The calculated ECC between

Ant 1 and Ant 8 coincides with the simulated value obtained from HFSS. The results of the analysis have validated that changing the weightings of the equiphase modes and the antiphase modes can improve the ECC effectively.

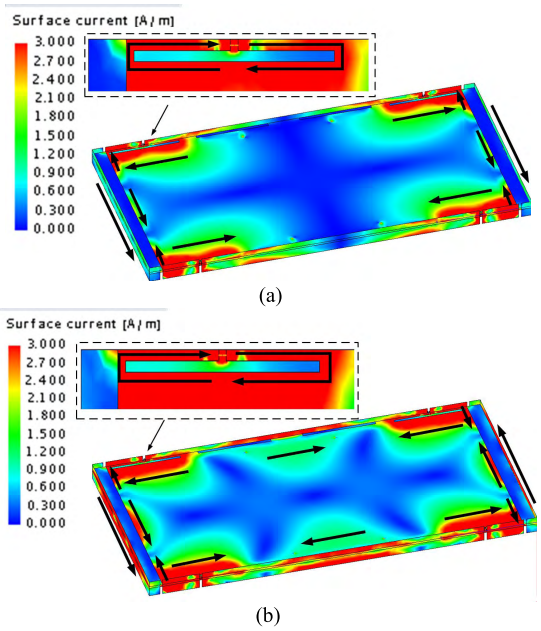

FIGURE 18. Modal current distribution of the proposed MIMO array. (a) Mode 11. (b) Mode 13.

To summarize the above findings, even though many identical modes are excited by two antennas, the CMT can also be used to improve the ECC between the two antennas. For the initial MIMO array, the ECC between Ant 1 and Ant 8 is undesirable. In order to improve the ECC between Ant 1 and Ant 8, the CMT is used to analyze Ant 1 and Ant 8. Although the main analyses conducted in this paper were between Ant 1 and Ant 8, the CMT can also be applied to analyze any other MIMO elements.

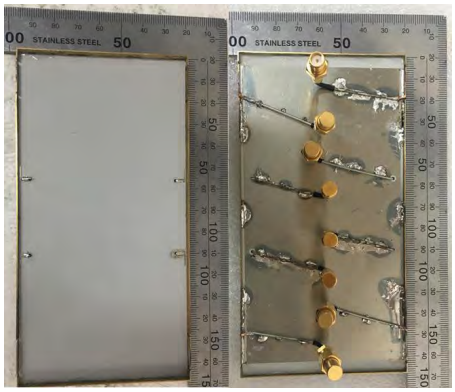

FIGURE 19. Photograph of the manufactured 8-port MIMO array.

IV. EXPERIMENTAL RESULTS

The proposed 8-port MIMO array has been fabricated and measured, and the fabricated MIMO array is shown in Fig. 19.

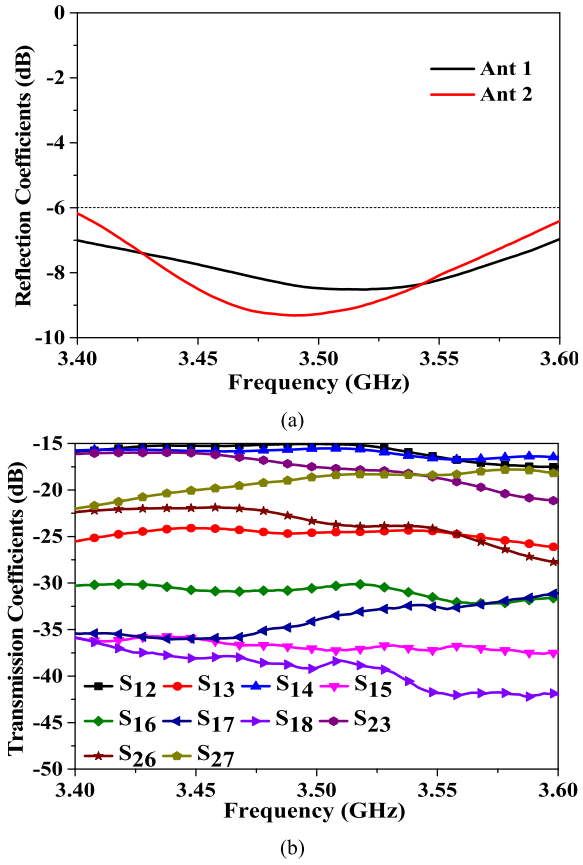

FIGURE 20. Measured (a) reflection coefficients and (b) transmission coefficients of the proposed MIMO array.

In order to reduce the effect between the metal bezel and SMA connectors, the SMA connectors are soldered at the central region of the ground. An Anritsu MS46322A vector network analyzer was used to measure the S parameters of the proposed antenna, and the results are shown in Fig. 20. As shown in Fig. 20(a), the 6-dB impedance bandwidth of Ant 1 and Ant 2 can cover the desired 3.4-3.6 GHz bands. In Fig. 20(b), the isolations between 8 antennas are better than

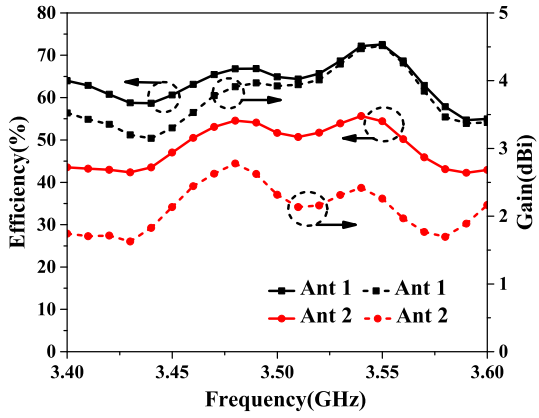

FIGURE 21. Measured efficiency and peak antenna gain of the proposed MIMO antenna.

TABLE 3. Comparison between the proposed and the referenced antennas.

Ref.	Bandwidth (GHz)	Isolation (dB)	Efficiency (%)	ECC	Antenna element size (mm×mm×mm)	Metal frame
[2]	3.4-3.6	Not mentioned	59-72(sim.)	Not mentioned	13.3×4×1.5 (IFA), 5×5×5 (corner-type CCE), 5×5×2 (center-type CCE)	without
[3]	3.4-3.6	> 10	40-60(mea. Array A), 30-52(mea. Array B), 30-52(mea. Array C)	<0.25 (Array A), <0.32 (Array B), <0.32 (Array C)	3×8 ×0.8 (Open slot)	without
[5]	3.4- 3.6	> 10	62-78(mea.)	<0.2	16.7×3×0.8 (Bending monopole strip)	without
[6]	3.4-3.6	>10	40-52(mea.)	<0.15	10×1×3.1(Gap-coupled loop antenna)	without
[7]	2.55-2.65	>12.5	48-63(mea.)	<0.15	31.2×1×5(dipole), 17.8×4×1(Open slot)	without
Proposed	**3.4-3.6**	**>15**	**42-73(mea.)**	**<0.16**	**27.3×1.2×0.8(slot antenna), 26.5×1×0.8 (loop antenna)**	**with**

Only 5G antenna module is considered for comparison.

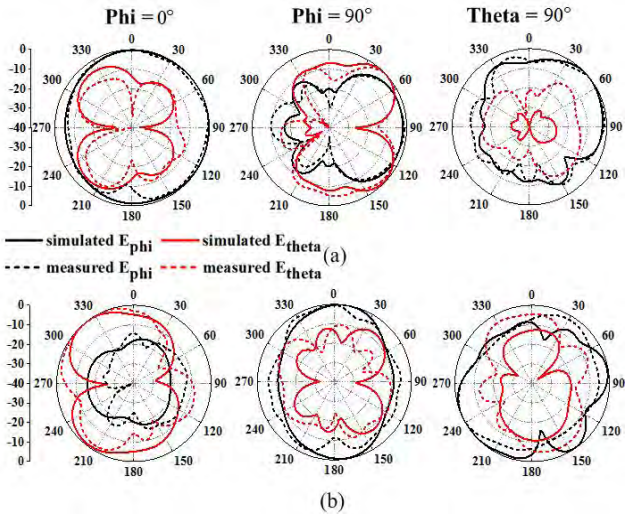

FIGURE 22. Measured and simulated normalized radiation patterns at 3.5 GHz. (a) Ant 1 excitation. (b) Ant 2 excitation.

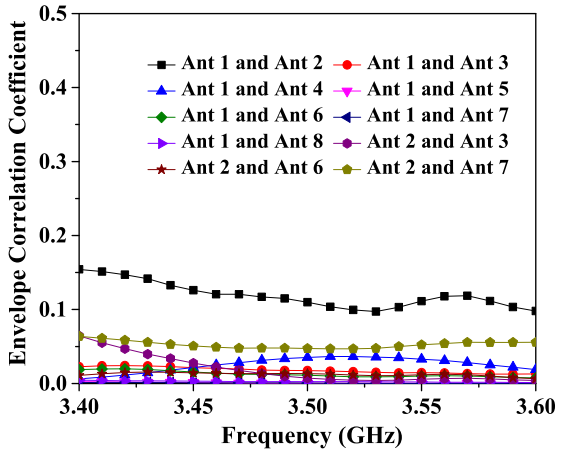

FIGURE 23. Measured ECCs of the proposed MIMO array.

15 dB. The measured S parameters agreed with the simulated ones.

The efficiency and radiation patterns are measured in a SATIMO microwave anechoic chamber and the results are presented in Figs. 21 and 22 respectively. The measured total efficiencies of the two antennas were approximately 42%-73% across the bands of interest (3.4-3.6 GHz). The measured peak antenna gains of the Ant 1 and Ant 2 are also depicted in Fig. 21. Over the frequency range of 3.4-3.6 GHz, the gain of Ant 1 was varied from about 3 to 4.5 dBi and the gain of Ant 2 was varied from about 1.6 to 2.7 dBi.

Fig. 22 shows the simulated and measured normalized radiation patterns of Ant 1 and Ant 2 at 3.5 GHz. During the measurement, when the pattern of one port is measured, the other ports are matched with 50 Ω. The simulated patterns are similar to the measured ones. Fig. 23 shows the measured ECCs that was calculated from the measured complex field patterns. The calculated ECC between Ant 1 and Ant 8 was lower than 0.005. This result proves that the method proposed in this paper can improve the ECC effectively. The slight differences between measured and simulated results may be due to the imperfect soldering of SMA connectors and the metal bezel, fabrication tolerance and the coupling between SMA connectors.

Finally, a comparison between the proposed MIMO array and some other 5G MIMO array is illustrated in Table 3. It is apparent that all of the 5G MIMO array listed in Table 3 are designed without metal frame. In addition, the MIMO arrays reported in [2], [6] and [7] are unable to apply to handset with metal frame. By comparing the isolation performance, the proposed MIMO array (consists of slot antennas and loop antennas) has demonstrated better isolation of > 15dB. It is also worth mentioning that the antenna element of the 5G MIMO array proposed in [5] is a three-dimensional bending monopole strip, and hence the excitation feed mechanism of this work is very different from [5].

V. CONCLUSION

In this paper, the applications of CMT in the frequency of multi-characteristic modes have been studied. As the existence of many significant modes is difficult for CMT to provide useful information, the situation when the modes (excited by two antennas) are overlapped has been studied. A new method is initially proposed to effectively analyze and improve the ECC of a multi-antenna system with multiple significant modes. The proposed method can provide useful physical insights and explain the physics behind undesirable ECC. According to the information provided by the proposed method, the solutions to improve ECC can be found much easier than before. A detailed and reasonable framework adopting the CMT to analyze a multi-antenna MIMO array with multi-significant modes is given. The same modes excited by two antennas can be categorized into two types, namely, equiphase modes and antiphase modes. The tradeoff of the equiphase modes and antiphase modes is first proposed and analyzed, and it was realized to be an efficient way to improve the ECC. Based on the theoretical derivation, the two parameters known as EC and AC can be calculated. From the findings, in order to achieve better ECC, it is recommended that the EC value should be made as close enough as to the AC value by changing the weightings of the equiphase modes and antiphase modes. The physical insights provided by the CMT can be used to reduce the difference between both EC and AC. The detailed framework for improving the ECC of 8-port 5G MIMO array by using the CMT has also been presented. According to the simulated and measured results, applying the CMT is beneficial in analyzing the frequency of MIMO array with multi-characteristic modes.

REFERENCES

[1] WRC-15 Press Release. (Nov. 2017). *World Radiocommunication Conference Allocates Spectrum for Future Innovation*. [Online]. Available: http://www.itu.int/net/pressoffice/press_releases/ 2015/56.aspx

[2] A. A. Al-Hadi, J. Ilvonen, R. Valkonen, and V. Viikari, "Eight-element antenna array for diversity and mimo mobile terminal in LTE 3500 MHz band," *Microw. Opt. Technol. Lett.*, vol. 56, no. 6, pp. 1323–1327, Jun. 2014.

[3] K. L. Wong, J.-Y. Lu, L.-Y. Chen, W.-Y. Li, and Y.-L. Ban, "8-antenna and 16-antenna arrays using the quad-antenna linear array as a building block for the 3.5-GHz LTE MIMO operation in the smartphone," *Microw. Opt. Technol. Lett.*, vol. 58, no. 1, pp. 174–181, Jan. 2016.

[4] K.-L. Wong, J.-Y. Lu, L.-Y. Chen, W.-Y. Li, Y.-L. Ban, and C. Li, "Antenna array in the smartphone for the 3.5-GHz MIMO operation," *Asia–Pacific Microw. Conf. (APMC)*, Nanjing, China, Dec. 2015, pp. 1–3.

[5] Y.-L. Ban, C. Li, C.-Y.-D. Sim, G. Wu, and K.-L. Wong, "4G/5G multiple antennas for future multi-mode smartphone applications," *IEEE Access*, vol. 4, pp. 2981–2988, 2016.

[6] K.-L. Wong, C.-Y. Tsai, and J.-Y. Lu, "Two asymmetrically mirrored gap-coupled loop antennas as a compact building block for eight-antenna MIMO array in the future smartphone," *IEEE Trans. Antennas Propag.*, vol. 65, no. 4, pp. 1765–1778, Apr. 2017.

[7] M.-Y. Li *et al.*, "Eight-port orthogonally dual-polarized antenna array for 5G smartphone applications," *IEEE Trans. Antennas Propag.*, vol. 64, no. 9, pp. 3820–3830, Sep. 2016.

[8] R. J. Garbacz, "Modal expansions for resonance scattering phenomena," *Proc. IEEE*, vol. 53, no. 8, pp. 856–864, Aug. 1965.

[9] Y. Chen and C. Wang, *Characteristics Modes Theory and Applications in Antenna Engineering*. Hoboken, NJ, USA: Wiley, 2015.

[10] D. Manteuffel and R. Martens, "A concept for MIMO antennas on small terminals based on characteristic modes," in *Proc. Int. Workshop Antenna Technol. (iWAT)*, Hong Kong, China, Mar. 2011, pp. 17–20.

[11] R. Martens, E. Safin, and D. Manteuffel, "Selective excitation of characteristic modes on small terminals," in *Proc. 5th Eur. Conf. Antennas Propag. (EUCAP)*, Rome, Italy, Apr. 2011, pp. 2492–2496.

[12] R. Martens and D. Manteuffel, "2-port antenna based on the selective excitation of Characteristic Modes," in *Proc. IEEE Int. Symp. Antennas Propag.*, Chicago, IL, USA, Jul. 2012, pp. 1–2.

[13] R. Martens and D. Manteuffel, "Systematic design method of a mobile multiple antenna system using the theory of characteristic modes," *Microw. Antennas Propag.*, vol. 8, no. 12, pp. 887–893, Sep. 2014.

[14] H. Li, Y. Tan, B. K. Lau, Z. Ying, and S. He, "Characteristic mode based tradeoff analysis of antenna-chassis interactions for multiple antenna terminals," *IEEE Trans. Antennas Propag.*, vol. 60, no. 2, pp. 490–502, Feb. 2012.

[15] H. Li, B. K. Lau, Z. Ying, and S. He, "Decoupling of multiple antennas in terminals with chassis excitation using polarization diversity, angle diversity and current control," *IEEE Trans. Antennas Propag.*, vol. 60, no. 12, pp. 5947–5957, Dec. 2012.

[16] H. Li, Z. T. Miers, and B. K. Lau, "Design of orthogonal MIMO handset antennas based on characteristic mode manipulation at frequency bands below 1 GHz," *IEEE Trans. Antennas Propag.*, vol. 62, no. 5, pp. 2756–2766, May 2014.

[17] C. Deng, Z. Feng, and S. V. Hum, "MIMO mobile handset antenna merging characteristic modes for increased bandwidth," *IEEE Trans. Antennas Propag.*, vol. 64, no. 7, pp. 2660–2667, Jul. 2016.

[18] R. Martens and D. Manteuffel, "Optimal placement of PCB-integrated diversity elements in a compact tunable handset antenna," in *Proc. 9th Eur. Conf. Antennas Propag. (EuCAP)*, Lisbon, Portugal, Apr. 2015, pp. 1–2.

[19] D. Poopalaratnam, K. K. Kishor, and S. V. Hum, "Multi-feed chassis-mode antenna with dual-band MIMO operation," in *Proc. IEEE Antennas Propag. Soc. Int. Symp. (APSURSI)*, Memphis, TN, USA, Jul. 2014, pp. 1427–1428.

[20] K. K. Kishor and S. V. Hum, "Multiport multiband chassis-mode antenna design using characteristic modes," *IEEE Antennas Wireless Propag. Lett.*, vol. 16, pp. 609–612, Jul. 2016.

[21] L. Qu, H. Lee, H. Shin, M.-G. Kim, and H. Kim, "MIMO antennas using controlled orthogonal characteristic modes by metal rims," *IET Microw., Antennas Propag.*, vol. 11, no. 7, pp. 1009–1015, Feb. 2017.

[22] A. Ghalib and M. S. Sharawi, "TCM analysis of defected ground structures for MIMO antenna designs in mobile terminals," *IEEE Access*, vol. 5, pp. 19680–19692, 2017.

[23] M. Ikram, R. Hussain, A. Ghalib, and M. S. Sharawi, "Compact 4-element MIMO antenna with isolation enhancement for 4G LTE terminals," *IEEE Int. Symp. Antennas Propag. (APSURSI)*, Fajardo, Puerto Rico, Jun./Jul. 2016, pp. 535–536.

[24] A. Ghalib and M. S. Sharawi, "Analyzing antenna effects on mobile chassis currents using theory of characteristic modes," *Microw. Opt. Technol. Lett.*, vol. 60, no. 8, pp. 1898–1905, 2018.

[25] E. Antonino-Daviu, M. Cabedo-Fabrés, M. Sonkki, N. M. Mohamed-Hicho, and M. Ferrando-Bataller, "Design guidelines for the excitation of characteristic modes in slotted planar structures," *IEEE Trans. Antennas Propag.*, vol. 64, no. 12, pp. 5020–5029, Dec. 2016.

[26] R. F. Harrington and J. R. Mautz, "Computation of characteristic modes for conducting bodies," *IEEE Trans. Antennas Propag.*, vol. 19, no. 5, pp. 629–639, Sep. 1971.

[27] R. F. Harrington and J. R. Mautz, "Theory of characteristic modes for conducting bodies," *IEEE Trans. Antennas Propag.*, vol. 19, no. 5, pp. 622–628, Sep. 1971.

[28] Sergey N. Makarov, *Antenna and EM Modeling with MATLAB*. Hoboken, NJ, USA: Wiley, 2002.

[29] S. M. Rao, D. R. Wilton, and A. W. Glisson, "Electromagnetic scattering by surfaces of arbitrary shape," *IEEE Trans. Antennas Propagat.*, vol. 30, no. 3, pp. 409–418, May 1982.

[30] J. Ethier, "MIMO antenna design using characteristic mode concepts," M.S. thesis, Dept. Elect. Eng, Ottawa Univ, Ottawa, KS, USA, 2008.

[31] R. Martens, E. Safin, and D. Manteuffel, "Inductive and capacitive excitation of the characteristic modes of small terminals," in *Proc. Loughborough Antennas Propag. Conf.*, Nov. 2011, pp. 1–4.

[32] F. A. Dicandia, S. Genovesi, and A. Monorchio, "Advantageous exploitation of characteristic modes analysis for the design of 3-D null-scanning antennas," *IEEE Trans. Antennas Propag.*, vol. 65, no. 8, pp. 3924–3934, Aug. 2017.

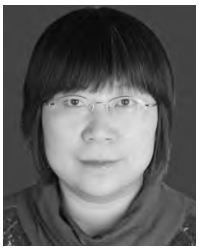

YING LIU (SM'17) received the B.Eng., M.S., and Ph.D. degrees in electromagnetics from Xidian University, Xi'an, China, in 1998, 2001, and 2004, respectively.

From 2006 to 2007, she was a Postdoctoral Researcher with Hanyang University, Seoul, South Korea. She is currently a Full Professor with the National Key Laboratory of Science and Technology on Antennas and Microwaves, Xidian University. She is also a Full Professor and the Director of the National Key Laboratory of Science and Technology on Antennas and Microwaves. She has authored or coauthored over100 refereed journal papers. She has also authored *Prediction and Reduction of Antenna Radar Cross Section* (Xi'an, China: Xidian University Press, 2010) and *Antennas for Mobile Communication Systems* (Beijing, China: Electronics Industry Press, 2011). Her research interests include antenna theory and technology, and the prediction and control of antenna RCS.

She is a Senior Member of the Chinese Institute of Electronics (CIE) and a Fellow of IET. She was a recipient of New Century Excellent Talents in University of the Ministry of Education for China, in 2011. She is a Reviewer of several international journals and serves as a TPC Member or a Session Chair for several IEEE flagship conferences. She serves as an Associate Editor for the IEEE Access.

AIDI REN was born in Chaohu, Anhui, China, in 1991. She received the B.Eng. degree in electrical engineering from Xidian University, Xi'an, China, in 2014, where she is currently pursuing the Ph.D. degree. Her current research interests include small antennas for handset device and MIMO antennas for wireless communications, especially for massive MIMO antenna for future 5G smartphones.

HU LIU received the B.S. degree in electronic information engineering and the M.S. and Ph.D. degrees in electromagnetic field and microwave technology from Xidian University, in 2012, 2015, and 2017, respectively. He is currently an Engineer with the Academy of Space and Electronic Information Technology, China. His current research interests include phased arrays and circularly polarized antenna design.

HANYANG WANG (SM'03) received the Ph.D. degree from Heriot-Watt University, Edinburgh, U.K., in 1995. He served as a Lecturer and an Associate Professor with Shandong University, Jinan, China, from 1986 to 1991. From 1995 to 1999, he was a Post-Doctoral Research Fellow with the University of Birmingham, Birmingham, U.K., and the University of Essex, Colchester, U.K. From 1999 to 2000, he was with Vector Fields Ltd., Oxford, U.K., as a Software Development and Microwave Engineering Consultant Engineer. He joined Nokia U.K. Ltd. , Farnborough, U.K., in 2001, where he was a Mobile Antenna Specialist for 11 years. He joined Huawei Technology Co., Ltd. after leaving Nokia, and he is currently the Chief Mobile Antenna Expert and the Head of the Mobile Antenna Technology Division. He is also an Adjunct Professor with the School of Electronics and Information Technology, Sichuan University, Chengdu, China. He holds over 40 granted and pending U.S./WO/PCT patents. His current research interests include small antennas for mobile terminals, patch and slotted waveguide antennas and arrays for mobile communications and airborne radars, and numerical methods for the solutions of electromagnetic radiation and scattering problems. He has authored over 80 refereed papers on these topics. He is a Huawei Fellow and an IET/IEE Fellow. He was a recipient of the Title of Nokia Inventor of the Year in 2005 and the Nokia Excellence Award, in 2011. He was also a recipient of the Huawei Individual Gold Medal Award, in 2012 and the Huawei Team Gold Medal Award, in 2013 and 2014, respectively. His patent was ranked number one among 2015 Huawei top ten patent awards. He is an Associate Editor of the IEEE Antennas and Wireless Propagation Letters. He is listed in Marquis Who's Who in the World and the International Biographical Center, Cambridge, U.K.

CHOW-YEN-DESMOND SIM (M'07–SM'13) was born in Singapore, in 1971. He received the B.Sc. degree from the Engineering Department, University of Leicester, U.K., in 1998, and the Ph.D. degree from the Radio System Group, Engineering Department, University of Leicester, in 2003. From 2003 to 2007, he was an Assistant Professor with the Department of Computer and Communication Engineering, Chienkuo Technology University, Changhua, Taiwan. In 2007, he joined the Department of Electrical Engineering, Feng Chia University (FCU), Taichung, Taiwan, as an Associate Professor, where he became a Full Professor, in 2012, and a Distinguish Professor, in 2017. He has served as an Executive Officer of the Master's Program with the College of Information and Electrical Engineering (Industrial Research and Development) and the Director of the Intelligent IoT Industrial Ph.D. Program, from 2015 to 2018. Since 2016, he has been serving as a Technical Consultant for SAG (Securitag Assembly Group), which is one of the largest RFID tag manufacturers in Taiwan. He is currently serving as the Head of the Department of Electrical Engineering and the Director of the Antennas and Microwave Circuits Innovation Research Center, Feng Chia University. He has authored or coauthored over 130 SCI papers. His current research interests include antenna design, VHF/UHF tropospheric propagation, and RFID applications. He is a Fellow of the Institute of Engineering and Technology (FIET), a Senior Member of the IEEE Antennas and Propagation Society, and a Life Member of the IAET. He was a recipient of the IEEE Antennas and Propagation Society Top 10 Outstanding Reviewer Award (IEEE Transaction on Antennas and Propagation) for five consecutive years between 2014 and 2018. He has also received the Outstanding Associate Editor Award from the IEEE Antennas Wireless and Propagation Letters, in 2018. He served as a TPC Member for the APMC 2012, the APCAP 2015, IMWS-Bio 2015, CSQRWC 2016, ICCEM 2017, APCAP 2018, and CIAP 2018. He has also served as the TPC Sub-Committee Chair (Antenna) for the ISAP 2014 and PIERS 2017. He was invited as the Workshop/Tutorial Speaker in APEMC 2015, iAIM 2017, and InCAP 2018, and an Invited Speaker of TDAT 2015, iWAT 2018, and APCAP 2018. He was a Keynote Speaker of SOLI 2018. He has served as an Advisory Committee of InCAP 2018 and has also served as the TPC Chair for the APCAP 2016 and the Chapter Chair for the IEEE AP-Society, Taipei Chapter, from 2016 to 2017. He has been the Founding Chapter Chair of the IEEE Council of RFID, Taipei Chapter, since 2017. He is currently serving as an Associate Editor for IEEE AWPL, IEEE Access, IEEE Journal of RFID, and the *International Journal of RF and Microwave Computer-Aided Engineering* (Wiley).